DRAFT
EIC PDR
October 2, 2024

Electron Ion Collider
Preliminary Design Report

Contributors:

E-C. Aschenauer[1], R. Ent[2], ADD NAMES AND INSTITUTIONS

[1]Brookhaven National Laboratory, USA
[2]Thomas Jefferson National Accelerator Facility, USA

Contents

List of Figures

List of Tables

multi-chapters

Chapter 8

Experimental Systems

8.1 Experimental Equipment Requirements Summary

Add text here.

8.2 General Detector Considerations and Operations Challenges

8.2.1 General Design Considerations

Add text here.

8.2.2 Backgrounds and Rates

Add text here.

8.2.3 Radiation Level

Add text here.

8.3 The ePIC Detector

8.3.1 Introduction

8.3.2 Particle identification

The requested discrimination capability (between two particle types) is conventionally defined as a Cherenkov angle separation greater than 3-σ, where σ is the mean angular resolution.

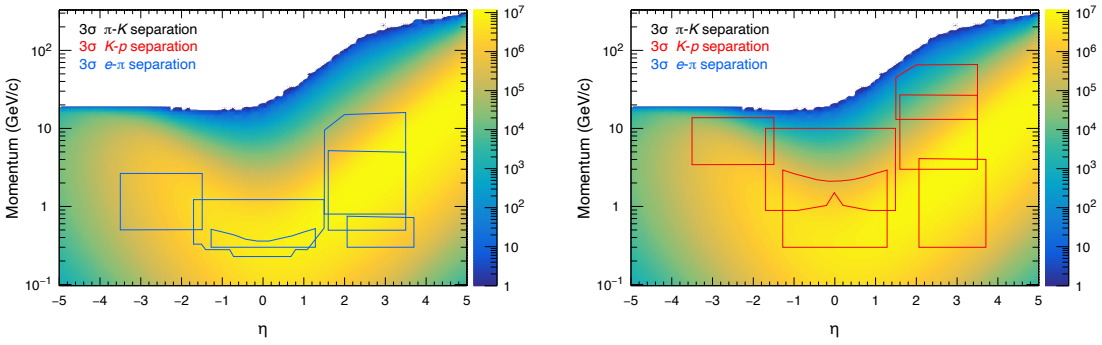

Figure 8.1: ePIC phase space coverage of the PID detectors

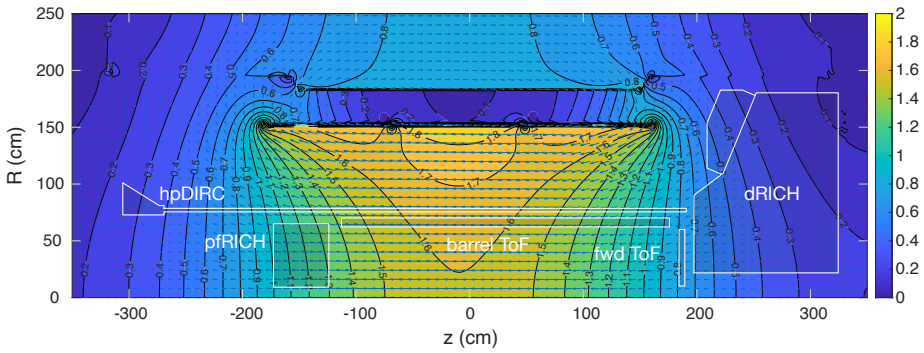

Figure 8.2: Map of the MARCO solenoid field with highlighted the PID detector volumes

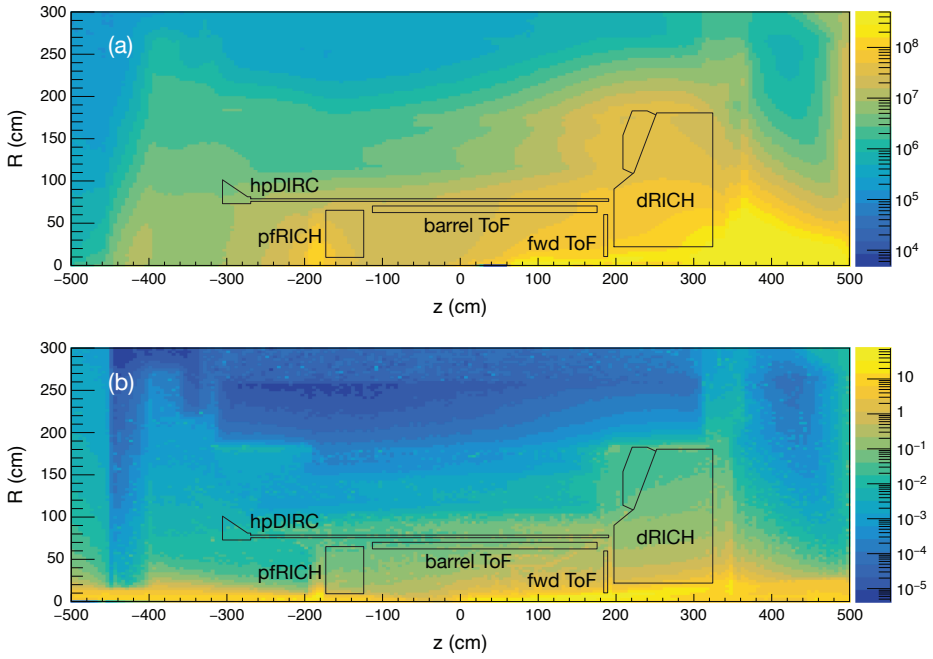

Figure 8.3: Estimated neutron fluence (top) and integrated dose (bottom) at ePIC with highlighted the PID detector volumes

8.3.2.1 The dual radiator RICH

Requirements The dual radiator Ring Imaging Cherenkov (dRICH) detector is part of the particle identification system in the foward (ion-side) end-cap of the ePIC detector and complements the forward time-of-flight system and calorimetry, see Fig. 8.1. The dRICH has to provide acceptance in the pseudo-rapidity range defined by the ePIC beam pipe and the barrel detector and to operate within the limited envelope allowed by the rest of the compact and hermetic ePIC detector. Distinctive features of the detector are: use of aerogel and gas radiators to extend the covered momentum range, usage of solid-state photomultiplier (SiPM) to ensure single photon detection capability in high and not-uniform magnetic field, non-conventional optics with curved active surfaces and compact readout electronics to fit into ePIC.

Requirements from physics: The dRICH is required to provide continuous hadron identification from $\sim$ 3 GeV/c to $\sim$ 50 GeV/c, and to supplement electron and positron identification from a few hundred MeV/c up to about 15 GeV/c. Such an extended momentum range imposes the use of two radiators, gas and aerogel, with a common imaging system to ensure compactness and cost-effectiveness. The radiator gas must ensure π/K separation at 3-σ level up to 50 GeV/c in the most forward region, namely for $\eta > 2$. The aerogel radiator must cover the intermediate momentum interval, bridging the upper limit of the time-of-flight ($\approx$ 2.5 GeV/c) to the Cherenkov threshold of the dRICH gas ($\approx$ 12 GeV/c). These requirements dictate the prescriptions on the refractive index and the radiator chromaticity in the sensitivity region of the photosensors. The dRICH has to provide open acceptance in the ePIC forward pseudo-rapidity range $1.5 < \eta < 3.5$. To provide proper light focalization within the due volume, the dRICH active area is located behind the shadow of the barrel detector and its support ring, close to the MARCO solenoid coils. In this region, see Fig. 8.2, the $\approx 1T$ strong and not-uniform ePIC magnetic field imposes the use of unprecedented detectors (SiPM).

Requirements from Radiation Hardness: The radiation sensitive components (sensor and front-end electronics) of the dRICH detector are concentrated in a region of moderate radiation level, below O(10^{11}) cm^{-2} n_{eq} of maximum integrated fluence where n_{eq} is a 1-MeV neutron equivalent particle, see Fig. 8.3. Close to the beam line, where the integrated dose can reach a value of 15 krad, only radiation tolerant materials reside like silica aerogel [3].

Requirements from Data Rates: The SiPM sensor features an intrinsic significant dark count rate, currently of the order of 50 kHz/mm^2 at room temperature, that indefinitely increases with the radiation damage. To mitigate this effect, the dRICH sensors are operated at low temperature (less than -30 C) and regularly annealed at high temperature (up to 150 C), in order to never exceed a maximum 300 kHz dark rate per channel. The latter value corresponds to a conservative limit taken to preserve the detector performance requirements for Physics and it is supported by present simulation studies that confirm the particle-identification capabilities of dRICH are unaffected.

Justification The specifications outlined above largely define the main technological choices: the momentum range dictates radiator refractive indexes that can be reliably met only by aerogel and gas, the ePIC environment, space and magnetic field, imposes sensor characteristics that can only be met by SiPM.

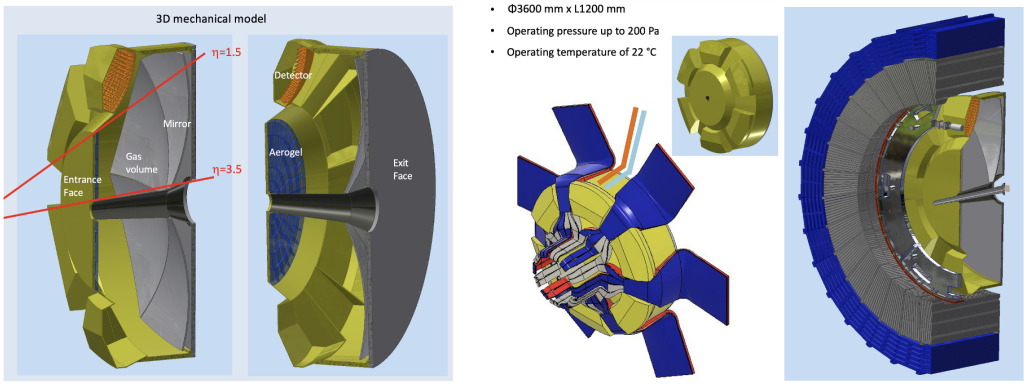

Figure 8.4: (Left) dRICH detector model with highlighted the major components. (Right) dRICH inside ePIC services lines at barrel HCAL end point.

Device concept and technological choice: The dRICH is a ring-shaped detector fitting inside the ePIC forward endcap, see Fig. 8.4. The essential components are a layer of aerogel radiator, a volume of gas radiator, and an array of mirrors focalising the Cherenkov light into compact areas instrumented with photo-sensors. The detector is designed in a modular way, with 6 sectors around the beam line of equivalent mirror set and detection area.

The aerogel radiator is a amorphous solid network of SiO_2 nanocrystals whose density regulates the refractive index and chromaticity [1]. The use of silica aerogel for RICH detectors is well established. It is available with refractive indices in the range 1.006–1.08 in between gases and liquids. The current manufacturing methods succeeded in improving the attenuation length Λ (λ = 400 nm) from 20 mm (aerogel used in HERMES) to 50 mm (aerogel for CLAS12 and BELLE-II). The selected aerogel radiator has refractive index n = 1.026 at $\lambda = 400\,nm$. The chromatic dispersion has been measured during the R&D phase to be $dn/d\lambda = XX\,nm^{-1}$ at 400 nm wavelength. Aerogel is typically produced in tiles of few cm thickness: in order to minimize edge effect, the dRICH tile side should be greater than 18 cm, approaching the word record value of 20 cm. The shape and surface flatness of the tiles are important parameters to consider for ensuring optimal PID performance. Typically, due to the fabrication process, aerogel tiles exhibit a slight meniscus shape. Measurements taken during the R&D phase on aerogel samples provided by Aerogel Factory Co. Ltd revealed deviations from the ideal parallelepiped shape by a few tenths of a millimeter, along with a thickness variation between the center and the edges of a similar magnitude. Based on the measurements conducted so far, this deviation from the ideal shape does not impact PID performance. Additionally, the manufacturer, Aerogel Factory Ltd (Chiba, JP), has confirmed that improvements in both flatness and thickness uniformity are feasible.

The selected reference gas radiator is hexafluoroethane (C_2F_6) (Appendix xxx), which matches the requirements being characterized by refractive index n = 1.00086 and excellent chromatic dispersion $dn/d\lambda = 0.2\,nm^{-1}$ at light wavelength $\lambda = 350\,nm$ [4].

The selected refractive indexes dictates a minimum thickness of 4 cm for the aerogel and O(1) m for the gas in order to ensure enough photon yield. Mirror focalisation is necessary to minimise the consequent uncertainty on the Cherenkov photon emission point. Being inside the detector acceptance, the mirror structure is made of carbon fiber reinforced polymer (CFRP) to ensure the necessary stiffness while being light. In order to preserve the Cherenkov angle information the mirror surface should have excellent optical quality, i.e. few nm roughness and better than 0.2 mrad angular precision (reflecting in a point-like image with more than 90% of the light intensity concen-

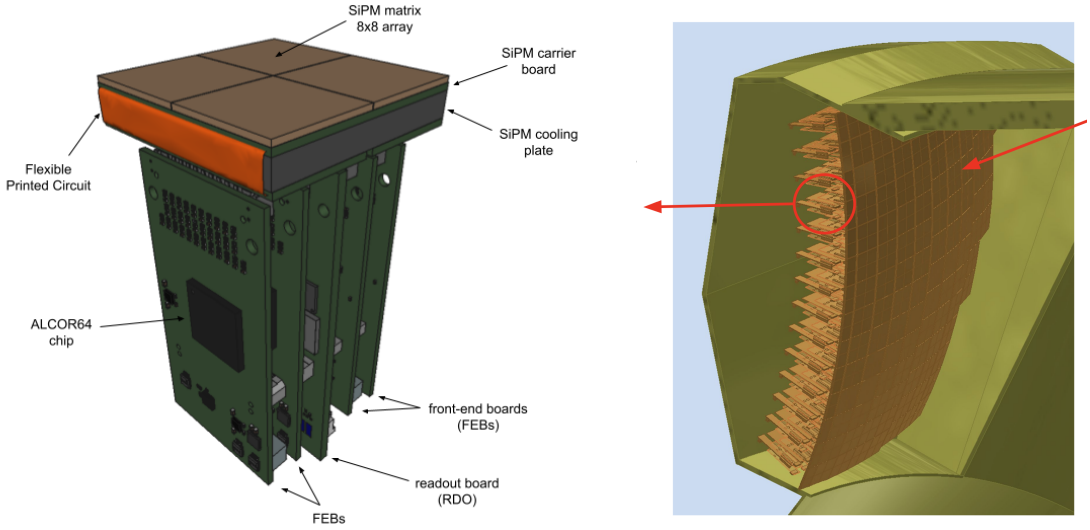

Figure 8.5: (Left) CAD model of the dRICH photodetector unit (PDU) module with its major components. (Right) dRICH detector box model with 208 PDUs forming a curved active surface.

trated in a disk smaller than 2.5 mm). The single mirror dimension is limited to a ≈ 1 m maximum diagonal when accounting for realistic forming mandrel and coating chamber dimensions. In the dRICH mirror array, the radius of curvature should be replicated within 1% of the nominal value.

The dRICH photon detector surface is shaped over a sphere of radius ~ 110 cm to best approach the 3D focal surface of the mirror array. The Silicon Photomultiplier (SiPM) sensor technology is selected for the photon detector. It ensures superior single-photon counting capability inside the ePIC magnetic field and compact dimensions suitable for tessellating a shaped active surface. The single SiPM sensor has a $3 \times 3\,\mathrm{mm}^2$ area to provide the necessary spatial resolution with an intrinsic time resolution better than 150 ps. The SiPM sensors are grouped into 8×8 arrays in a buttable arrangement to minimize the dead area, which are eventually mounted side-by-side to form a 16×16 array defining the 256 channels of the dRICH photodetector unit (PDU). The selected front-end ASIC is ALCOR, a 64-channel chip with coupling and rate capability optimized for SiPMs, and a ToT architecture with better than 50 ps LSB [1] resolution in order the SiPM-ALCOR readout chain could achieve an overall time resolution better than 200 ps RMS. To minimize the volume within the dRICH envelope and to maximize the active area, the photodetector is organized in compact photodetector units (PDU). The PDU integrates 256 SiPM channels with the ALCOR TDC readout provided by four front-end boards (FEB), one readout board (RDO) to interface with the ePIC data aquisition (DAQ) and detector control (DCS) systems. In addition, the PDU is designed to allow sub-zero cooling of the SiPMs as well as high-temperature annealing operations. Figure 8.5 (left) shows the conceptual design of the PDU and its main components. The present dimensions of the PDU concept are approximately $52 \times 52 \times 140\,\mathrm{mm}^3$.

Figure 8.6: (Left) dRICH aerogel model. (Right) dRICH mirror model [placeholder].

[1] Least Significant Bit

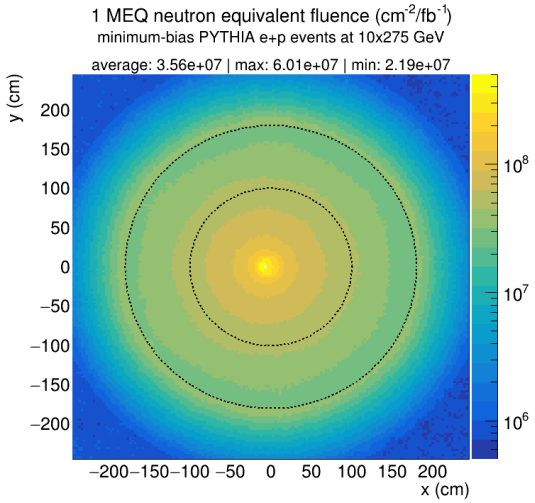

Figure 8.7: Transverse map of the expected 1-MeV equivalent neutron fluence per 1 fb^{-1} of integrated luminosity in e+p interactions at the maximum EIC center-of-mass energy at the location of the dRICH photodetector ($210 < z < 260$ cm). The average, maximum and minimum values within the region of the dRICH photodetector ($100 < R < 180$ cm, indicated by the dashed lines) are reported.

Subsystem description:

General device description:
Because at ePIC the electron and hadron beam collide at an angle of XX mrad, the common beam pipe cross-section is off-axis at the dRICH location and increasing in area with the distance from IP, imposing an asymmetric layout of the inner components, see Fig. 8.6. The aerogel wall is composed by five rings of tiles, each shaped in order to fit inside a 0.2 mm thin aluminum supporting structure. In each sector, focalization is provided by a compound of five mirrors covering a total area of about 2 m^2 with an optimized radius of curvature around 2200 mm. Six independent spherical active surfaces with curvature radius around 1100 mm, each made of 208 PDUs for a total of 53k readout channels, are mounted inside detector-boxes that provide thermal insulation, cooling for the electronics and connections to the services. Given the gas radiator open volume, the Cherenkov photons can be reflected into different detectors depending on the parent charged particle kinematics. The aerogel and photo-detector are separated from the radiator gas by transparent septa, and immersed in a dry (e.g. purged N_2) atmosphere to minimize contaminant absorption and prevent moisture formation. The mirrors are supported by a light carbon fiber structure that is mechanically decoupled from the vessel and allows fine alignment adjustments by means of pizezo-electric motors.

Sensors:
The silicon photomultiplier (SiPM) [5, 6] is chosen as the sensor technology for the dRICH photodetector. The main baseline specifications demand sensors with a 3×3 mm^2 single-channel active area, single photon detection over a broad spectral range from 300 to 900 nm and very high overall photodetection efficiency $> 40\%$ at the peak sensitivity wavelength $400 < \lambda_{peak} < 450$ nm (see Table 8.4 in Additional Material for the full list of the baseline parameters and specifications of the SiPM sensor devices for the dRICH photodetector). SiPMs fulfil the dRICH requirements being cheap and versatile devices with excellent photodetec-

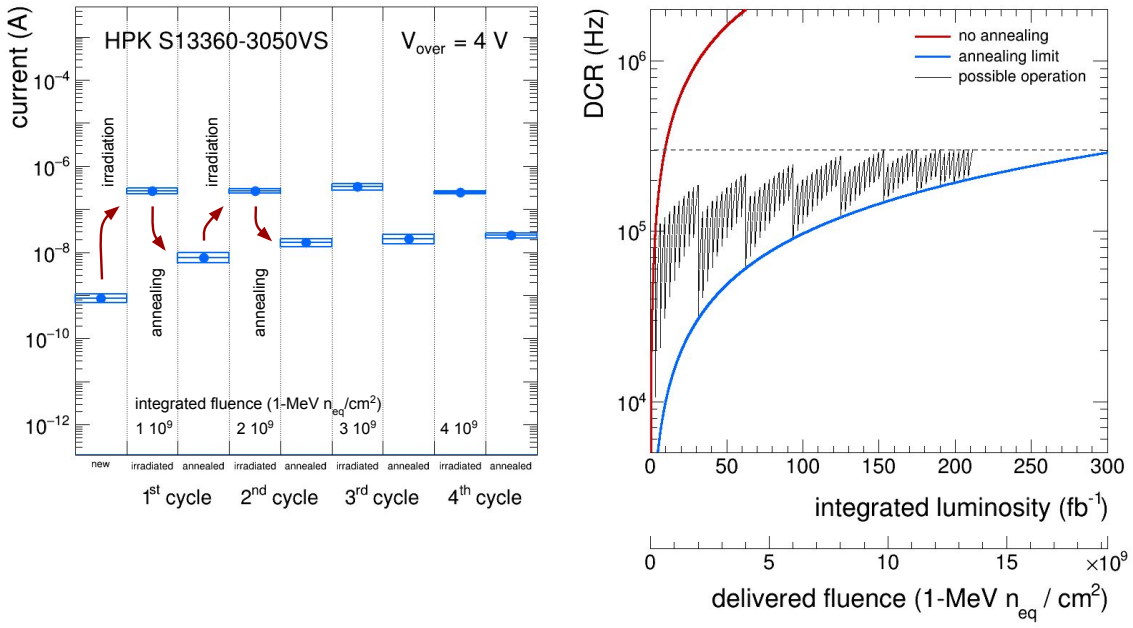

Figure 8.8: (Left) Dark current measurements on sample SiPM sensors for the studies of repeated irradiation-annealing . (Right) Projected increase of the DCR of SiPM as a function of the integrated luminosity (delivered fluence). The "no annealing" and the "annealing limit" curves show the limits of possible operations. The dashed line indicate the desired maximum DCR threshold.

tion efficiency (PDE) and time resolution. Their single-photon performance is unaffected by high magnetic fields [7, 8], which makes SiPM the only photosensor that can efficiently operate in the field configuration at the dRICH photodetector location in the ePIC experiment, see Fig. 8.2. SiPM sensors on the other hand have very high dark count rates (DCR) and are not radiation tolerant. The DCR in SiPM is mostly of thermal origin and it reduces significantly by lowering the SiPM temperature, typically halving every 7-10°C in new sensors [9]. Radiation damage in SiPM is mainly due to displacement damage in silicon, which causes a significant DCR increase and reduces the effectiveness of cooling [10]. At the moderate radiation levels expected at the location in the dRICH, no significant change in the SiPM parameters (PDE, gain, quenching resistor R_{quench}, pixel capacitance C_{pixel}, breakdown voltage V_{break}) is observed [11]. SiPM cooling is important to keep the DCR low and it becomes crucial after radiation damage [12], as the increase in DCR would be such to make SiPM unusable as single-photon detectors, otherwise. In the dRICH, the SiPMs will be operated at subzero temperature of T = -40°C, or lower. A cooling block is placed in thermal contact with the back-side of the printed-circuit board hosting the SiPMs (carrier board). Cooling fluid in the cooling block will be circulated through a closed loop by a dynamic temperature control system circulating thermostat to regulate and maintain the SiPMs at low temperature The circulating thermostat system will also be used to circulate fluid at high temperature (T = 100°C, or higher) to provide heat during SiPM annealing. Therefore a low-viscosity silicone fluid is particularly suitable for cold and heat transfer. The radiation damage on SiPMs increases moderately with the integrated luminosity. At the location of the dRICH photodetector a maximum (average) fluence of Φ_{eq} = 6.0 (3.6) 10^7 cm^{-2}/fb^{-1} 1-MeV equivalent neutrons (n_{eq} in the following) is expected from e+p interactions at the highest center-of-mass energy

of the EIC (Figure 8.7). Beam-induced background from proton beam-gas events at 35 kHz are expected contribute with a maximum (average) of Φ_{eq} = 3.7 (1.6) 10^6 cm^{-2}/fb^{-1} n_{eq} at the location of the dRICH photodetector, bringing the total maximum (average) expected radiation damage to Φ_{eq} = 6.4 (3.7) 10^7 cm^{-2}/fb^{-1} n_{eq}. As shown by the "no annealing" curve in Figure 8.8 (right), the SiPM DCR is expected to increase with the integrated luminosity at a rate of 31.8 (18.6) kHz/fb^{-1}, reaching a DCR of 300 kHz after an integrated luminosity of approximately 9.5 (16.1) fb^{-1}. These values are based on measurements performed on Hamamatsu S13360-3050 sensors operated at V_{over} = 4 V at T = $-30°$C., more details in Section **??**.

Annealing of SiPMs can be achieved exploiting the Joule effect []. When a SiPM is forward biased, the microcells composing the device behave as directly polarized diodes connected to their quenching resistors. The current flowing through the resistors eventually heat up the entirety of the sensor. In the dRICH, SiPM annealing will be performed up to temperatures of T = 150°C in "forward-bias mode". The actual annealing temperature and annealing time will be tuned during detector operations according to the DCR reduction needs and available experiment down time. The "forward-bias mode" approach can cure approximately 97% of the radiation damage. It is therefore expected that a residual irreducible radiation damage (residual DCR) will build up during the dRICH lifetime. As shown by the "annealing limit" curve in Figure 8.8 (right), the SiPM residual DCR is expected to increase with the integrated luminosity at a rate of 950 (560) Hz/fb^{-1}, reaching a residual DCR of 300 kHz after an integrated luminosity of approximately 310 (530) fb^{-1}. In the dRICH, SiPM annealing will be performed with a technical implementation of the "forward-bias mode" which needs to be integrated both into the SiPM power-supply system, the front-end and control electronics, cooling and the temperature monitoring system. As previously mentioned, the circulating thermostat system used for low-temperature operation of the SiPM will be operated in heating mode to warm up the SiPM cooling plate during high-temperature annealing. This will allow one to perform the "forward-bias annealing" by delivering a lower current to the SiPM, as as fraction of the heating power is delivered by fluid. Nonetheless the required power to perform "forward-bias annealing" at once over the full dRICH detector is excessively large. Therefore annealing operations will be segmented in space and time across the dRICH detector and will be performed during periods with no Physics beam and depending on the DCR needs. As can be see from Figure 8.7 the sensors closer to the beam line will experience a radiation damage almost a factor 3 larger than those father from the beam line and will likely require a more frequent annealing. The "possible operation" curve in Figure 8.8 (right) shows a potential scenario for the DCR evolution for SiPM sensors closer to beam pipe (worst case). This is based on an operation model where more frequent (every $\sim$ 3 fb^{-1}) softer annealing cycles at lower temperature and/or of shorter duration, delivering a DCR reduction of 10×, are interleave by less frequent (every $\sim$ 30 fb^{-1}) full annealing cycles to reduce DCR as much a possible. A limit in the operation scenario is reached when the annealing is not capable to keep the DCR below the desired threshold or when the annealing frequency become too high. As it can be seen from Figure 8.8 (right), beyond an integrated luminosity of $\sim$ 200 fb^{-1} to keep the DCR below the 300 kHz threshold requires to perform full annealing cycles every $\sim$ 5 fb^{-1}, which is not obviously a practical operation scenario anymore. Some or all of the SiPM sensors might be needed to be replaced at that stage with new ones or with SiPM sensors of improved performance and radiation hardness in a future upgrade of the dRICH photodetector. One has to keep in mind though that the 300 kHz limit is a conservative value that is connected to the present level of dRICH reconstruction and could be relaxed in future. Moreover, the model shown in Figure 8.8 (right) is based on measurement on Hamamatsu S13360-3050 sensors operated at V_{over} = 4 V in a climatic chamber at T = $-30°$C. Possible SiPM operation in ePIC at a lower V_{over} of 3 V and at a lower T of $-40°$C will allow one to achieve lower DCR overall.

FEE:
The ALCOR (A Low Power Chip for Optical Sensor Readout) ASIC, developed by the electronics laboratory of INFN Torino, is the baseline option for the readout of the dRICH SiPM sensors. The main goal of ALCOR is to provide single-photon time tagging of the incoming signals, while being able to cope with the SiPMs inherently high DCR: a maximum DCR value of 300 kHz/ch is expected before an annealing cycle is performed. A good time resolution, better than 200 ps RMS, is required to perform DCR suppression via time gating at both hardware and software levels. ALCOR is a mixed-signal ASIC comprising 64 channels arranged in a 8x8 pixel matrix. The ASIC includes in-pixel signal amplification, conditioning and digitization, with a fully digital output using 8 LVDS DDR Tx links operating at a clock frequency of 394.08 MHz, a multiple of the EIC clock frequency. The architecture of one ALCOR pixel is displayed in the left panel of Fig. 8.9. The amplifier input stage is a low impedance current conveyor based on a regulated common-gate topology suited for sensors with large capacitance such as SiPM sensors. The versatile front-end is able to work with positive or negative input polarity signals and includes four gain settings and two discriminators with 6-bit DAC programmable thresholds. Each channel also incorporates 4 low-power TDCs based on analogue interpolation providing precise timestamping with a 20-40 ps time bin. This architecture allows for single-photon time tagging and includes Time-over-Threshold (ToT) or Slew-Rate (SR) measurements for time walk correction. ALCOR is designed in a 110 nm CMOS technology and the power consumption is about 12 mW per channel. The ASIC adopts a time-based readout: every signal above the threshold is processed by the pixel control logic and digitized, without any external trigger. This data-push architecture matches well with the ePIC streaming readout approach, in which the detectors will be read out continuously. Limited by the 6.3 Gb/s bandwidth of the ASIC data transmission links, ALCOR can operate at a maximum event rate of about 2.4 MHz per channel in time-tagging mode and 1.2 MHz per channel when operating in ToT and SR mode. A programmable hardware shutter, implemented inside ALCOR pixel digital logic, can be enabled to filter out-of-time DCR and provide a significant bandwidth reduction to the system. The time window of interest is controlled off-chip by the RDO and can be adjusted using in-pixel programmable delays to compensate timing offsets among the 64 channels. With a time window of approximately 2-3 ns, considering that the EIC bunch crossing period is about 10.15 ns, data can be reduced by a factor of 3 or 5. One important point is that the shutter will be needed only when DCR becomes higher due to SiPMs taking radiation damage over time. Therefore, the first period of ePIC data taking can be used to optimize the shutter calibration. The ASIC will be integrated inside a BGA package, providing a compact and robust solution to be assembled on the FEB. A 16×16 mm^2 flip-chip ball grid array (FC-BGA), with 256 balls and 1 mm ball pitch, is the option chosen for the ASIC packaging since it offers more interconnections and better performance w.r.t. standard packaging techniques and matches well with the pixel-matrix geometry of the ALCOR ASIC. A 3D model of the FEB is shown in the right panel of Fig. 8.9. Each FEB hosts one ALCOR BGA device and several components to ensure a stable and safe operation of the system. Linear regulators are employed to provide clean power supplies to the ALCOR ASIC and are coupled to I2C interface and current monitors to control the regulators and prevent potential damage from over-current conditions. The FEB also incorporates a dedicated PCB section for SiPMs bias voltage routing and also a circuit to enable the SiPM forward-biasing when annealing cycles are carried out. AC-coupling between the SiPM sensors and ALCOR inputs has been chosen to isolate them when the SiPMs are operated in forward bias. Several connectors, mounted on the FEB, provide the interface towards the RDO and the other FEB boards of the same PDU as well as towards the SiPMs carrier board and the LV-HV services.

Other components:

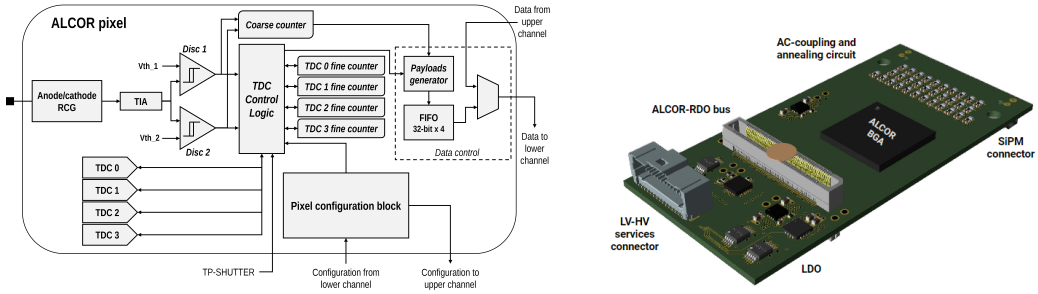

Figure 8.9: (Left) Block diagram of ALCOR pixel. (Right) 3D model of the dRICH FEB.

The radiator gas in the RICH vessel is controlled by the gas radiator system (Fig. 8.10). Its main tasks are, during detector operation, (i) providing well controlled pressure conditions in the 12 m^3 RICH vessel to avoid relevant pressure difference at the vessel walls and at the fused silica windows; (ii) removing oxygen and water vapor contaminates, in order to prevent building up impurities due to air leaks entering the gas system; (iii) performing detector vessel filling with hexafluoroethane before a data taking period and radiator gas recovery at the end of the period; the filling/recovery is from/to the storage tank. The main components of the radiator gas system are two oil-free compressors, working in parallel, which continuously extracts gas from the vessel at constant rate in order to ensure the gas circulation, a pressure sensor installed on top of the radiator vessel for continuous monitoring of the internal relative pressure and to dictate the opening level of a flow control valve on the input line, adjusting the opening so to preserve the relative pressure inside the vessel. Oxygen and water vapor traces are removed by filtering cartridges with molecular sieves and Cu-catalyst, which are permanently in series in the circulation system. The vessel is flushed with nitrogen during the shutdown periods. Nitrogen and hexafluoroethane separation during filling and recovery is under study and two options can be envisaged: (i) the use of osmosis via dedicated membranes or (ii) via a two-step procedure: replacing nitrogen with carbon dioxide and then performing distillation at -35^oC. Hexafluoroethane is a greenhouse gas and, therefore, the residual C_2F_6 present in the nitrogen/carbon dioxide cannot be vent out: it must be collected and trapped for disposal with a dedicated recovery system. The control of the whole radiator gas system is performed via a Programmable Logic Controller (PLC). More details are provided in Appendix xxx.

Performance

For each recorded dRICH hit, the photon path is reconstructed taking into account the charged particle trajectory and the focalising optics of the detector, in order to provide an estimate of the Cherenkov angle at the emission point. The combined information of all the Cherenkov photons associated to a charged particle concur to a precise determination of its velocity (beta) and, knowing the momentum from the ePIC spectrometer, its mass. The dRICH model is part of the ePIC simulation framework and allows complete performance studies taking into account quality of the track reconstruction, bent trajectories (by magnetic field) and multiple scattering. To bypass the complexity of such a framework, some specific study can be anyway performed with private or simplified simulation chain. The laboratory characterization and the numerous test-beams have provided detailed inputs for modeling in a realistic way the single components and global detector response. In the dRICH, the contributions to the single-photon (SPE) angular resolution have a different weight depending on the radiator. The dRICH has been designed in order to keep most of the contributions to the SPE angle resolution below 0.5 mrad, see Fig. 8.11, a value dictated by

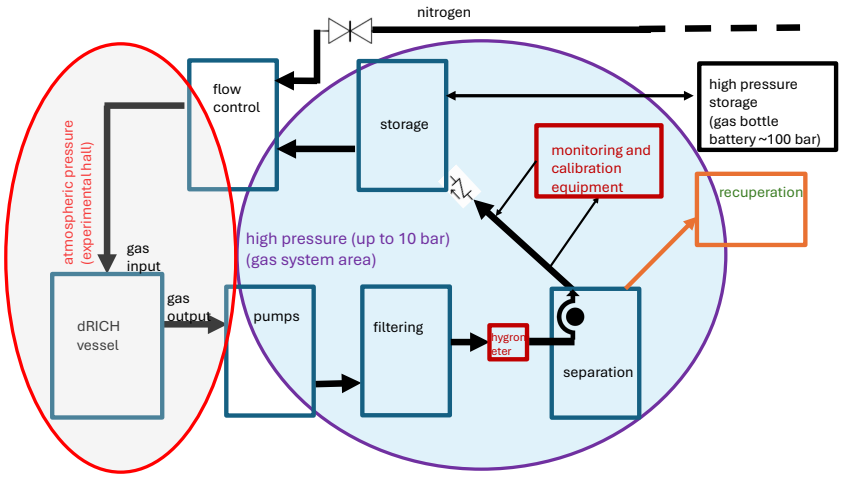

Figure 8.10: Block diagram of the dRICH gas system [graphically, a preliminary version].

the tiny Cherenkov angle difference between pions and kaons at 50 GeV/c in the radiator gas. The single SiPM readout channel has been limited to 3×3 mm^2 area. The MARCO coils and the dRICH position has been optimized in order to minimize the bending inside the radiator gas volume. The tracking resolution is assumed to cope with the same constrain. Note that combining N photons the angular precision scale with a maximum $N^{-1/2}$ factor only in case of a completely uncorrelated information, a condition that is not valid for the bending and tracking contributions. The uncertainty on the emission point is not an issue for a few cm layer of aerogel, but is critical for a 1 m long gas volume, expecially within the limited space available in ePIC for the optics: this remains the major contribution to the SPE resolution of the radiator gas despite the mirror focalization and the curved dRICH detector surface. As the present model assumes a single radius for the dRICH mirros, optimized for the forward rapidity region to boost the high-momentum reach, the resolution worsens with the polar angle increase. This is not a problem, because the average particle momentum decrease as well loosing the performance requirement. The chromatic error is well under control for gas but is the largest contribution to the angular resolution for the aerogel. This derives from the intrinsic nature of the radiator in conjunction with the quantum efficiency characteristic of the photosensor. The chromatic uncertainty limits the aerogel momentum reach to something above 15 GeV/c, a value well above the Cherenkov threshold of kaons in gas, high enough to provide the wanted overlap between the measured ranges of the two radiators.

The number of emitted photons varies with the pseudo-rapidity due to the different path of the particle within the radiators. The mean number of recorded photons is about 18 for the radiator gas and 12 for the aerogel for a particle with momentum well above the Cherenkov threshold. In average, few charged particles per event are expected to hit the detector, see left panel of Fig. 8.12. With a proper pattern recogition and photon path reconstruction, the information of the two radiators can be combined to extend the momentum coverage of ePIC PID from the TOF $\approx$ 2.5 GeV/c upper momentum limit to above 50 GeV/c, see central panel of Fig. 8.12. In the forward direction with optimized focalization, an identification efficiency greater than 95 % at a corresponding 5 % percent mis-identification probability, is achieved, see right panel of Fig. 8.12. As expected from the resolution study, the momentum reach is reduced with the pseudo-rapidity, in accordance wth the kinemartics of the particles expected from physics reactions.

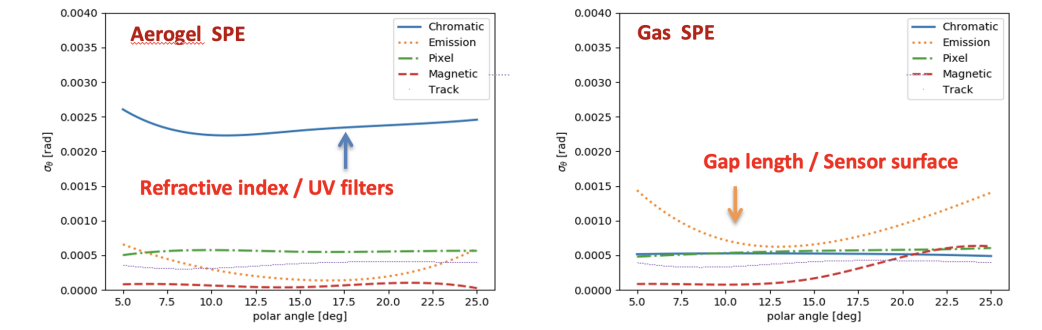

Figure 8.11: (Left) Contributions to the single-photon angular resolution for aerogel. (Right) Contributions to the single-photon angular resolution for radiator gas.

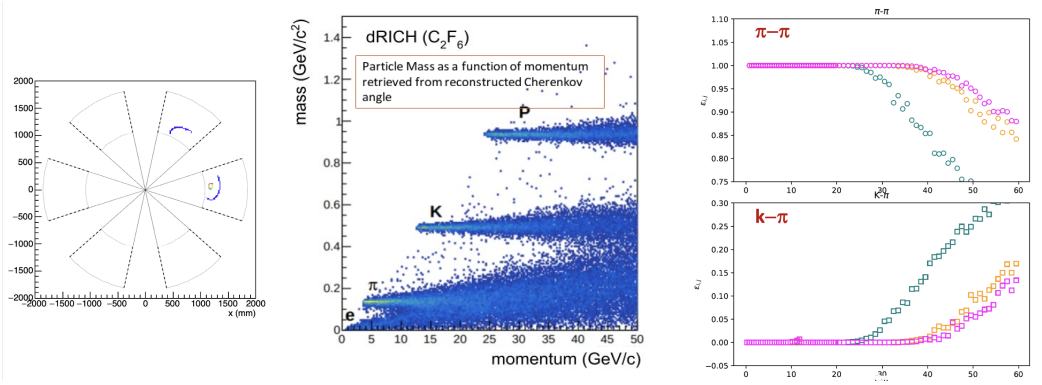

Figure 8.12: (Left) Event display. (Center) Reconstructed mass vs momentum. (Right) Pion identification efficiency and pion to kaon mis-identification probability as a function of momentum in three bins of rapidity.

Implementation

Services:

The dRICH services are grouped into power lines for sensors, electronics and slow control monitors, gas lines for the radiator gas volume, the aerogel inert gas volume, and cooling lines for the

Name	Voltage (V)	Current (A)	Channels	Boards	AWG gauge
Analog	1.4	10.0	312	39	10
Digital low	1.4	8.5	312	39	11
Digital high	2.7	6.0	312	39	12
Master panel	5.0	5.2	6	1	13
SiPM bias	64.0	1.3	12	2	19
Annealing	12.0	3.2	1248	156	15

Table 8.1: List of the voltage services to the dRICH electronics, indicating the number of primary power-supply channels and boards as well as the cross-section of the cables (AWG). The number of power-supply boards is defined assuming to use commercial 8-channel low-voltage boards.

sensors and electronics. Table 8.1 shows a list of the power services for the dRICH photodetector. 18 19" wide/8U mainframes (approximately $50 \times 40 \times 70$ cm^2 each) capable to host 16 boards each are needed to accommodate the low-voltage and high-voltage boards. The primary power-supply channels will serve multiple modules at the same time, with a typical grouping of 1024 SiPM channels. Nonetheless, further segmentation is implemented on the detector electronics, reaching a low-voltage power segmentation of 64 SiPM channels and a high-voltage power segmentation of 32 SiPM channels. The circulating thermostat system should be capable of circulating approximately 50 l/min of fluid at a maximum pressure of 1.5 bar in a broad temperature range (from -60°C to 120°C). Possible commercial systems are available, but more time is needed to better investigate the options. It is expected that a potential circulating thermostat system with the desired characteristics will require space in the experimental hall for a volume of approximately $1.3 \times 0.8 \times 1.6$ m^3. Manifolds are needed to split the fluid from the thermostat into 6 loops, each feeding one dRICH photodetector box. A solution without manifold and 6 smaller independent thermostat unit for each dRICH sector will be investigated as a possible optimization. Insulated pipes will be needed to transport the fluid from the thermostat to the detector, and back. The insulation must guarantee no frost and no water condensation on the pipes when operating at the lowest temperatures and is also required to limit transport losses in heating/cooling capacity. Cooling for the front-end electronics is required to remove the approximately 15 kW of heat generated by the dRICH photodetector ($\approx$ 2.5 kW in each of the six photodetector boxes). Force-air circulation in the boxes with diffusers are being studied as a possible effective solution. It is important that the air-cooling system for the FEE electronics provides dry air with a dew point of T = -70°c or lower, well below the SiPM operating temperature. A system based on forced circulation of gaseous nitrogen might be well suited also to ensure an inert environment inside the detector boxes. Gaseous nitrogen will also be used to maintain the aergoel in a clean and inert environment. The radiator gas system and its related monitoring equipment require a surface of about 15 m^2, in order to host 5 racks of instrumentation, the gas storage tank and a support for the spectrophotometer. This surface includes the space needed by the operators. Various sections of the gas system operate at a 2-3 bar pressure, while the cell to measure and monitor the gas transparency operates at 10 bar. Some gas bottles at typical high pressure (100-150 bar), organized in a battery, have to be included to provide the radiator gas at filling and house it when recovered. The pipelines connecting the gas system to the vessel are 70 m long with a diameter of 10 cm.

Subsystem mechanics and integration:
The dRICH structure can be described by two disks, one entrance window of 0.9 m radius supporting the aerogel radiator and one exit window of 1.8 radius mounting the mirror system, connected by two ring-shaped structures, one shell that mounts the six detector boxes and one inner pipe surrounding the ePIC beam pipe. All the elements are made in composite materials. The pipe and shell are made by a carbon fiber reinforced polymer (CFRP) bulk to provide support strenght. The two windows are a sandwich of two carbon fiber skins and a core honeycomb to limit the material budget to about 1% of radiation length. The shell and detector boxes are shaped in order to allow the passage of all the services of the inner barrel detectors, see left panel of Fig. 8.13. The dRICH services are concentrated on the shadow of the detector boxes and do not interfere with the routing of the others. A dedicated scaffolding would be realized to allow the installation of the detector, and the roll-in and roll-out movements to the service position without interference with the beam pipe to preserve the beam vacuum, see central and right panel of Fig. 8.13. The dRICH is suspended inside ePIC via brakets connected to the HCAL barrell.

Calibration, alignment and monitoring:
Dark counts in SiPMs are indistinguishable from photon-induced signals and owing the large SiPM

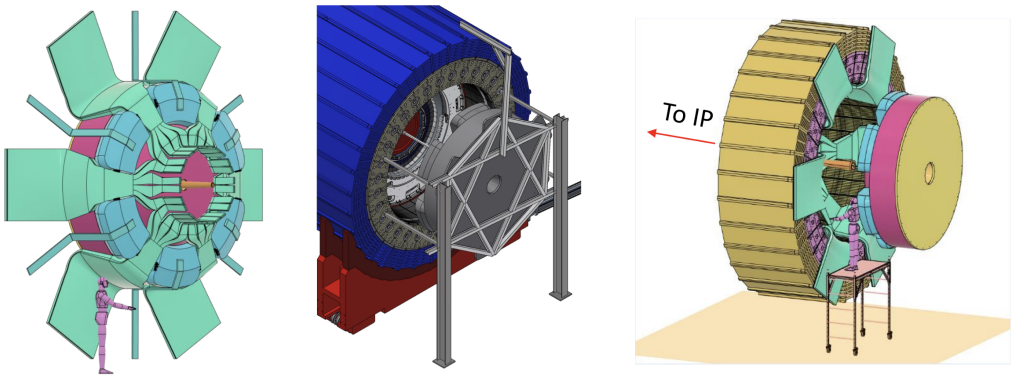

Figure 8.13: (Left) Service routing around the dRICH. (Center) Installation tool. (Right) Maintenance position.

DCR there is no need of a dedicated system to evaluate the functioning of any given readout channel. A measurements of the DCR as a function of the front-end electronics discrimination threshold can provide information on the signal amplitude. This technique can be used at different bias voltages. Using solely the dRICH readout system it is possible to measure the signal amplitude as a function of the bias voltage, hence to obtain information on sensor functioning and its breakdown voltage at different operation conditions. Timing calibration of the SiPM sensors can be achieved with a picosecond pulsed laser light system. The light from the laser is brought inside the dRICH volume via optical fibres. The light from the laser directly impinges on a diffuser that eventually illuminates the full area of one dRICH photodetector sector. At least one laser-fibre-diffuser system is needed for each dRICH sector. The time delay due to the different path of photons from the diffuser to the SiPM that detects the light is known and can be corrected to achieve a relative calibration of the times of SiPMs within the same sector. Absolute timing calibration can then be achieved with collision data. Samples particles from physics reactions can be used to perform fine adjustment of the calibration costants. Electron particles identified by other ePIC subsystems can be used to correct residual misalignment or calibrate the radiator refractive index thanks to the saturated Cherenkov rings. Known particles from meson decays (Λ, ϕ, K_S, ...) identified by kinematics criteria can be used to verify the parameters of the dRICH reconstruction and the consequent PID performance. The calibration and monitoring equipment of the radiator gas and gas system (Appendices xxx, yyy, ...) includes a set of temperature sensors placed inside the dRICH vessel and equipment on-line in the gas circulation loop. A commercial hygrometer and a commercial oximeter, a transparency measurement system by a commercial spectrophotometer equipped with a high pressure ($\approx$ 10 bar) cell and a Jamin interferometer setup complete the set of the equipment. The interferometer, complemented with temperature and pressure sensors, will provide in real-time the refractive index of the gas in the vessel. The refractive index measurement has a twofold role: during filling/recovery, it monitors the hexafluoroethane level in the vessel, during operation it will provide in real time the refractive index of the radiator gas to make possible quasi on-line data reconstruction as foreseen in the ePIC streaming read-out model.

Status and remaining design effort:

R&D effort:

SiPM sensors. A station has been realized to characterize the SiPM sensors inside a climatic chamber to control the working temperature, see left panel of Fig. 8.14. The readout chain is based on ALCOR to reproduce the ePIC configuration. Such a station allowed detailed

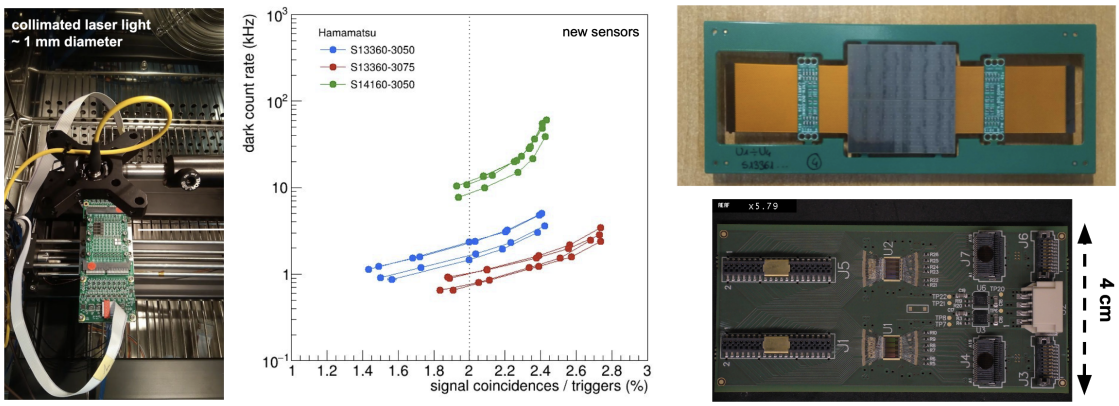

Figure 8.14: (Left) Test stand for SIPM characterization. (Center) Performance comparison between different SiPM models. (Right) Prototype version of the SiPM carrier board (top) and FEB (bottom).

performance comparison between SiPMs of different manufacturers and types, and different ageing due to radiation and annealing, e.g. see central panel of Fig. 8.14. The R&D results on photosensors reported here are those obtained with Hamamatsu S13360-3050 sensors operated at V_{over} = 4 V in a climatic chamber at T = $-30°$C, unless otherwised specified. Nonetheless, the qualitative features of the results are valid also for other types of sensors. Irradiation tests and laboratory measurements on SiPM candidate samples show that after irradiation with a fluence of $\Phi_{eq} = 10^9$ cm^{-2} n_{eq} the DCR increases by approximately 500 kHz with respect to the DCR measured when new [13]. The dark current and the DCR of irradiated SiPM decreases by almost two order of magnitudes when placed in a thermostatic chamber at T = 150°C for 150 hours ("oven annealing"). Further tests performed to simulate a realistic experimental situation where SiPMs experience repeated irradiation and annealing cycles (see left panel of Figure 8.8) show that each irradiation cycle produces a consistent DCR increase (approximately 500 kHz for a 10^9 cm^{-2} n_{eq} irradiation) and a consistent residual DCR (approximately 15 kHz for a 10^9 cm^{-2} n_{eq} irradiation) remains after an "oven annealing" cycle. The fraction of damage cured by the "oven annealing" cycle is of approximately 97% of each newly-produced irradiation damage. The residual damage of 15 kHz/10^9 n_{eq} builds up after each irradiation-annealing cycle and seems to be irreducible within the details of this annealing protocol. The "oven annealing" protocol is not a practical approach for a central-barrel detector in a collider experiment, because of the limited access and because it would entail the removal of the sensors from the photodetector to place them the thermostatic chamber to perform annealing. Irradiation tests and laboratory measurements show that the "forward-bias annealing" mode can cure radiation-induced damage on SiPM (see left panel of Figure 8.15) to the same effectiveness level as the one measured for the "oven annealing" with a residual damage of approximately 3%. The benefit of the "forward-bias annealing" is significant: an extended SiPM sensors lifetime that can be achieved over the delivered radiation damage without the need to directly access the detectors in the experimental cavern. The fraction of damage, measured as dark current reduction, depends on the annealing temperature and the duration of the annealing. Higher temperatures and longer annealing times lead to more effective annealing. On the other hand, a limit seems to be reached already at T = 150°C and annealing at a higher temperature of T = 175 C does not lead to improved current reduction. Self-heating of the SiPM happens also when reverse biased, although given that the reverse I-V characteristics of SiPM is non-linear and depends

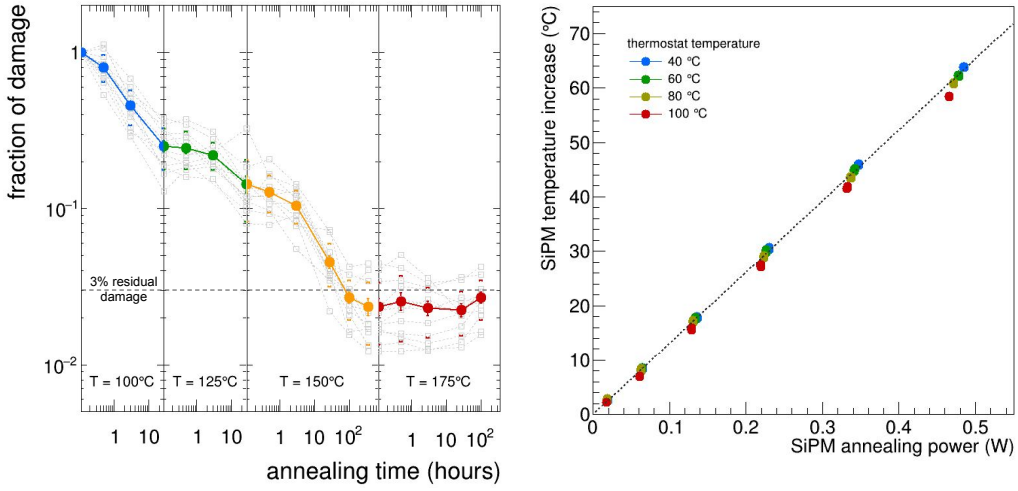

Figure 8.15: (Left) Fraction of residual irradiation damage measured on multiple SiPM candidate samples after "forward-bias annealing" cycles at increasing temperature and integrated annealing time. The measurements are shown for individual sensors (gray points) and as averages (coloured points, uncertainty of the average and RMS are indicated on the plot). (Right) Temperature increase of the SiPM sensor with respect to the temperature of the SiPM carrier board as a function of the "forward-bias annealing" power at different temperature values of the circulating thermostat system.

on the illumination state, currents can increase with less control making the reverse-bias annealing intrinsically more dangerous than forward-bias annealing. Laboratory measurements performed so far show that one can increase the temperature of the SiPM with respect to the temperature of the SiPM carrier board proportionally to the power delivered by the forward-bias current. Figure 8.15 (right panel) shows that, as expected, the increase of SiPM temperature linearly depends on the annealing power and it is the same at different values of circulating thermostat temperature. It is therefore sufficient to monitor the temperature of the SiPM carrier board and deliver the needed annealing power to have control of the SiPM temperature during "forward-bias annealing" and keep the process safely under control. Laboratory measurements reported here are performed in an open environment at room temperature. With the circulating thermostat temperature set at T = 100°, we reach a SiPM annealing temperature of T = 150° with approximately a power of 0.5 W/sensor, which corresponds to a forward-bias current of approximately 60 mA/sensor. With the SiPM placed in a closed environment as the in dRICH photodetector box, one would expect a lower power needed that will be measured during detector construction. Laboratory measurements of the variation of the SiPM PDE as a function of the annealing temperature and annealing time show that for annealing temperatures up to T = 150° there is no observation of a significant degradation of the PDE up to annealing times of 150 hours. On the other hand, annealing at a temperature of T = 175° seem to cause a degradation of the transparency of the silicone protective window of the SiPM, which causes a decrease in the PDE to approximately 80% of the initial value after 150 hours. As already discussed, annealing at temperatures higher than T = 150° does not bring any advantage for what concerns DCR reduction. More studies will be done, but at the time of writing annealing at T = 150° can be considered safe for the expected dRICH operations.

FE Electronics. ALCOR has been extensively used within the ePIC dRICH Collaboration since 2021. The current version of ALCOR incorporates 32 channels, arranged in a 8×4 pixel matrix. It has been tested coupled to different SiPM models assessing its single-photon time-tagging capability and time resolution. A prototype version of the SiPM carrier and FEB board have been developed, see right panel of Fig. 8.14. The SiPM carrier provides electrical connections via thin kapton cables in order to bypass the sensor cooling plate. The prototype FEB hosts two 32-channel ALCOR chips which are directly wire-bonded on the PCB. It has been designed using specifications close to the ones for the final FEB, i.e. having the same dimensions and incorporating the same number of channels (64). It is served by a master-logic board that provide bias control and temperature monitor. These boards have been extensively used for the 2023-2024 dRICH activities, including two successful beam tests. ALCOR has been tested for radiation hardness with results showing only some small degradation on the TDC performance after a total ionizing dose (TID) of 300 krad, which is O(100) times the expected TID in ePIC. These results confirm that the technology is sufficiently radiation tolerant to be used in the ePIC dRICH environment and that no special design techniques have to be adopted for the new version of ALCOR. The single-event upset (SEU) cross section has been measured to be $3.3{\cdot}10^{-15}$ cm^2/bit for the pixel configuration registers and $8.5{\cdot}10^{-14}$ cm^2/bit for the periphery configuration registers, which is significantly higher because these registers are not triplicated in the current version of ALCOR. From these results we can expect a mean time between failure due to SEU of about 190 hours for the entire dRICH detector.

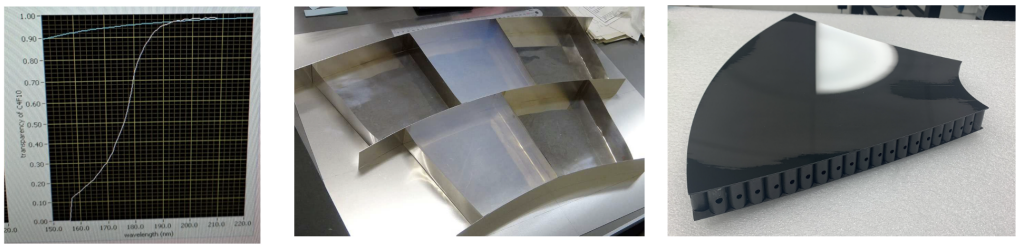

Figure 8.16: (Left) C_2F_6 measured transmittance. (Center) Aerogel large tiles assembling as obtained at BELLE-II [1]. (Right) Mirror demonstrator with an optimized dRICH core structure.

Radiator gas. The transparency in the near-UV benchmark region (most sensitive to the gas quality and contaminants) has been measured with a monochromator at CERN, resulting in values above 98% for a 1.6 m coloumn of gas at wavelengths grater than 200 nm, see left panel of Fig. 8.16. The measurement has been done with a gas that was stored into bottles for about 4 years, indicating an excellent preservation with time.

Aerogel. Several measurements were performed to optically characterize the aerogel. The transmittance of silica aerogel is a measure of how much light passes through the material without being absorbed or scattered. Silica aerogel consists mostly of air. Indeed, it has a unique structure made of a three-dimensional network of interconnected nanopores, with diameters ranging from 2 to 50 nm, which allows visible light to pass through the material with minimal scattering or absorption. Specifically, in aerogel, light undergoes Rayleigh scattering, which is the elastic scattering of light by particles much smaller than the wavelength of the light. The transmittance is typically highest in the near-infrared region, where the absorption of radiation by the silica network is minimal. Its dependence on the radiation wavelength is usually defined by the Hunt formula [14] which assumes a λ^4-dependence of Rayleigh scattering cross section. In silica aerogel, the low absorption is due to the absence

of impurities or defects in the silica network that could trap and dissipate the energy of the photons. Additionally, silica aerogel can be hydrophobic or hydrophilic. The tiles tested are highly hydrophobic, which means that they repel water and other liquids. This property helps to maintain the material's transparency even in humid or wet conditions. The aerogel scattering and absorption capability can be assessed through the transmission length as follows: $1/\Lambda_T = 1/\Lambda_{scat} + 1/\Lambda_{abs}$.

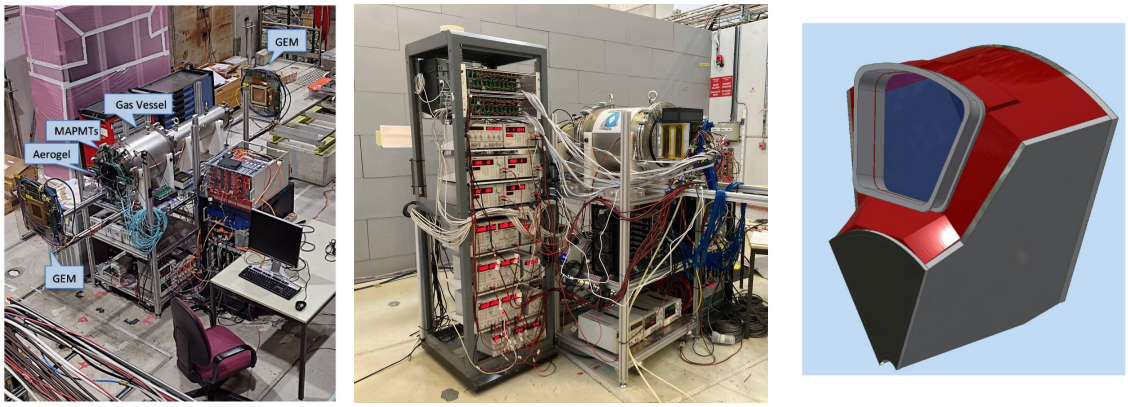

Figure 8.17: (Left) Baseline prototype with reference detector at the SPS-H8 beam line of CERN. (Center) First ePIC-drive detector box under test at the PS-T10 beam line of CERN. (Right) Real-scale prototype model mimicking the basic dRICH construction unit (sector).

We have characterized several 10×10 cm^2 and 5×5 cm^2 aerogel tiles produced as a spin-off the BELLE-II development in a broad range of refractive indexes. Table 8.5 reports a list of the tested samples, where for each tile its refractive index and expected thickness in the thinnest point of its meniscus geometry are reported. On each tile transmittance was measured on 15 different sampling points, to provide information on the dependence of the transmittance on the thickness as well as on the light wavelength (in a range from 250 to 800 nm). The maximum discrepancy along the tile is of the order of $\approx 0.3\%$, the transparency homogeneity is quite good. Transmittance as a function of the wavelength of a single tile was considered as the average of the transmittance value at each sampling point. The average transmittance was fitted by the extended Hunt formula suggested in [14] to extract scattering and absorption lengths. The results are presented in Fig. 8.21 for a tile with n = 1.03, which shows that the transmission length is nearly equal to the scattering length, whereas the absorption length is considerably higher. Therefore, the contribution of absorption can be considered negligible. A comparison of the results from all the tested tiles can provide valuable insights into the impact of the refractive index on the optical properties of the aerogel, see Fig. 8.22. The transmittance measurements reveal that the tiles with a refractive index close to n=1.03 exhibit higher transmittance length values at 400 nm compared with tiles of higher or lower refractive index, see Fig. 8.23. In the metrology laboratory at CERN, the thickness and flatness of the tile have been also measured. The measurement has been executed on a tile with n = 1.03 using the touch probe system (force applied = 2 g). The measuring system is the LEITZ PMMC with $\pm$ 0.3 μm of precision. There is a variation in thickness from the center to the edges, of the order of 0.4 mm, and a different planarity in the two faces, one 0.7 mm, the other 1.27 mm. In general the tiles have the shape of a dome.

Mirror. A mid-size demonstrator (of 60 cm diagonal) has been realized with dRICH specifications, see right panel of Fig. 8.16. The CFRP core structure has been optimized for preserving the surface shape accuracy and a light body: it adopts the light LHCb structure in the

center, and the stronger CLAS12 structure on the edges. Before coating, the point-like source image test measures a D0 value, that represents a global surface quality estimator, of 1.8 mm, better than the specification of 2.5 mm. The same test indicates a radius of 2254.1 mm, slight above the request to be within 1% of the nominal 2200 mm value.

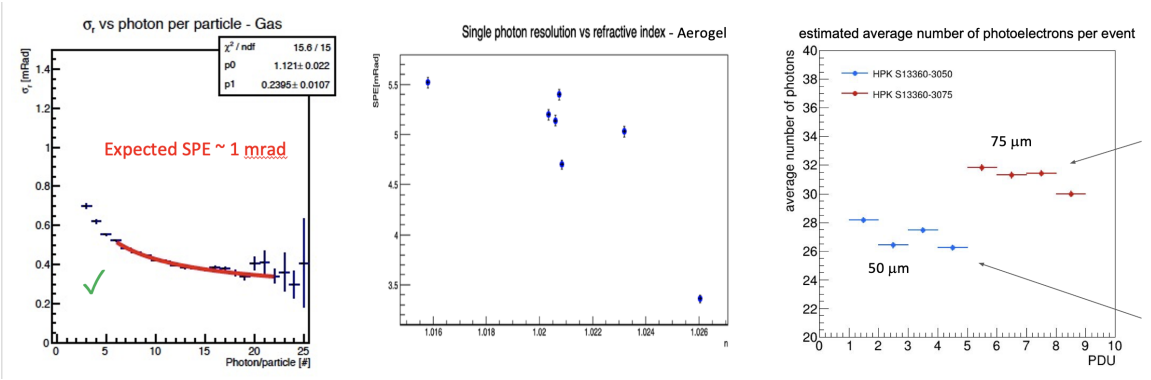

Figure 8.18: (Left) Cherenkov angular resolution obtained for C_2F_6 as a function of the recorded number of photons. The SPE values is consistent with expectations. (Center) SPE angular resolution measured on aerogel as a function of the refractive index. The expected resolution is obtained for an index greater than n=1.025. (Right) Comparison in photon yield of sensor with different SPAD size. All the measurements are obained with the dRICH prototype.

Prototyping. A baseline prototype has evolved in time to serve the dRICH R&D development for few years, see left panel of Fig. 8.17. The gas vessel is a cylinder made of vacuum standards, to allow an efficient and safe gas exchange. The entrance flange can mount an external dark box separated from the inner gas volume by a UV-transparent lucite foil (or quartz window). An aerogel tile with possible additional UV filters, plus an array of alternative sensors and readout electronics, can be inserted into the dark box. Two mirrors inside the vessel have optimized focal lenghts to image the Cherenkov light from the two radiators onto the limited active surface. The major achievements obtained during several test-beams have been the validation of the dual-radiator concept, the validation of the C_2F_6 gas radiator (see left panel of Fig. 8.18), the optimization of the aerogel refractive index (see central panel of Fig. 8.18), the performance study of the SiPM-ALCOR readout chain (see right panel of Fig. 8.18), and the development of an EIC-driven readout plane. A partially equipped EIC-driven plane has been realized in time for the October '23 test-beam with Hamamatsu S13360-3050 SiPM sensors of standard 50 μm pixel pitch, see left panel of Fig. 8.19. The plane has been complemented for the test-beam in May 2024 with sensors of 75 μm pixel pitch, to verify the potential benefit in timing and photon detection efficiency. This has allowed for the first time a full ring coverage, an essential requirement for precise radiator performance study and effective signal over background study, see central panel of Fig. 8.19. An effective interplay between the two radiators at intermediate energies has been demonstrated, see right panel of Fig. 8.19. The new detector box has allowed a preliminary study of the thermal gradients and possible effects on the gas performance, indicating that the possible temperature gradient of few degrees induced into the gas volume by the cool sensor plane can be largely mitigated by a gas re-circulation or by a double window.

E&D status and outlook:

A new version of the ALCOR ASIC is currently being designed to extend the number of channels to 64 and integrate the chip inside a BGA package, aiming to enhance the scalabil-

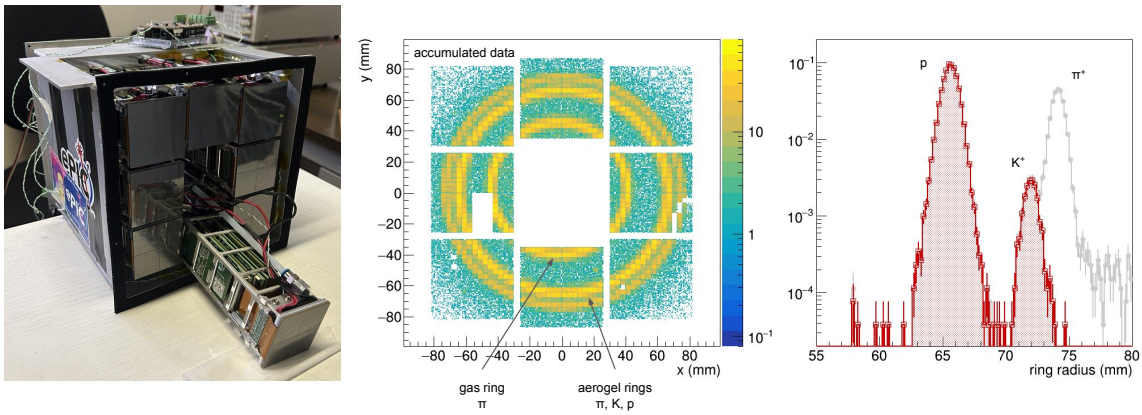

Figure 8.19: (Left) Prototype PDU and assembled detector plane. (Center) Cumulated ring imaging. (Right) dual-radiator interplay for a mixed hadron beam at 10 GeV/c. After the gas information is used to tag pions, an effective separation between kaon an proton is provided by the aerogel.

ity of the readout system and meet specific EIC-driven requirements. The ASIC package will use FC-BGA technology with 256 balls and 1 mm ball pitch. Since no re-distribution layer (RDL) is available for the 110 nm technology in which ALCOR is fabricated, a dedicated 10-layer 1.27 mm thick substrate in bismaleimide-triazine (BT) resin material is currently being designed. This BT epoxy provides a more advanced and reliable solution w.r.t. many FR4 grade materials, while being also commonly available from multiple vendors. In particular, its higher thermal conductivity and lower z-axis coefficient of thermal expansion (CTE) values make it more suited to cope with repeated thermal cycles, in which CTE mismatches may induce mechanical stress on the BGA solder joints. The new version of ALCOR will also include some internal design revisions. A programmable hardware shutter is being implemented to filter out-of-time DCR and thus significantly reduce the data throughput. The asynchronous digital shutter is implemented in ALCOR pixel logic using the external test-pulse signal and will be provided by the RDO board. Inside the ASIC programmable delay chains, with 4 configuration bits at channel-level (LSB $\simeq$ 350 ps) and at the chip periphery (LSB $\simeq$ 100 ps), allow the compensation of the offsets between different pixels and columns. In addition, the front-end will feature an increased bandwidth amplifier to improve the system time resolution while keeping the same power consumption and also an hysteresis circuit in the discriminator stage to avoid unwanted re-triggering on the SiPM signals slow tail, occurring when operating with very low thresholds. To improve its overall SEU tolerance, the new version of the ASIC will implement triple modular redundancy (TMR) also for the periphery registers as well as error-correcting Hamming encoding for the finite-state machines (FSM). Further irradiation tests are foreseen in 2025-2026 on ALCOR final version to fully validate the front-end electronics in terms of radiation tolerance for all of its components. The tape-out is scheduled during the first months of 2025. A thorough electrical characterization of this version of ALCOR, the first one assembled in a BGA package and including all the features required for the dRICH application, will be carried out to validate its new functionalities and measure its performance in order to complete the E&D activity and go ahead with ASIC mass production which is foreseen in 2026.

The development of the final front-end boards takes advantage of the work done for the prototype version in terms of space constraints, readout scheme and components selection. To finalize their layout several design optimization are required: define the best segmentation

and routing to provide the bias voltage to the SiPMs, optimize the AC-coupling circuitry between ALCOR and the SiPM sensors, include the annealing circuit required to operate the SiPMs in forward-bias, distribute the power lines and optimize the control and monitor protocols. In addition, all components that will be mounted on these boards need to be tested to verify their radiation hardness. The design of the final version of the SiPM carrier, FEB and master-logic boards will be completed in 2025 while the mass production is expected during 2026.
For the radiator gas, it is required to complete the design of the gas system and finalize the layout of the monitoring equipment. Each of these activities assumes an engineering study and its validation by laboratory studies. The remaining E&D activity is expected to be completed by the end of 2026.
An increase of the aerogel tile volume is instrumental to minimize the edge effects and contain the cost. During the R&D phase, tiles with side up to 15 cm and thickness up to 2 cm were realized. A feasibility study is ongoing to increase these limits towards a side of 20 cm or a thickness of 3 cm to support the successful assembling scheme adopted at BELLE-II, see central panel of Fig. 8.16. The aerogel production efficiency should be evaluated in conjunction with the optical quality obtained. This engineering work is expected to take time and not be completed before the end of 2026.
Coating of the CFRP mirror substrate should be realized and compare with the benchmark performance obtained with the same materials at CLAS12. This work will be completed by mid 2025.
A real-scale prototype is being realized with composite materials and a realistic geometry (mimicking a dRICH sector). This is instrumental to validate the mechanical elements and study the assembling details (e.g. of transparent septa), the mechanical stability, the gas tightness, and the thermal aspects. One of the major goals of the real-scale prototype is also to reproduce the final ePIC working conditions, mount an extended readout plane with the designed RDO board, operate demonstrators of the optical components as results of the ongoing developments, and optimize the performance in a realistic off-axis optics configuration. To this end, a test-beam is planned for mid 2025.

Other activity needed for the design completion:
Slow control, interlock and the calibration LED/laser system design is not started yet.

Status of maturity of the subsystem:
The R&D activity has been focused on the most innovative aspects of the detector that present technological challenges. These are the SiPM for single-photon detection in a strong magnetic field, a compact readout electronics to fit into the ePIC envelope and the use of two radiators to extend the momentum reach. The remaining effort is substantial, but is connected to more consolidated technologies, with possibly the only exception of the gas separation system for the peculiar C_2F_6 gas.

Environmental, Safety and Health (ES&H) aspects and Quality Assessment (QA planning:
Standard slow-control and interlock procedures will be implemented to control power and cooling while monitoring gas flow, humidity and temperature. The cooling system is complemented by a buffer tank to allow air flow and heat removal from the detector boxes in case of a failure of the recirculating system. The gas volume is maintained at +1 mbar with respect the atmospheric pressure on the top, with a consequent +5 mbar overpressure defined by the hydrostatic pressure of the radiator gas on the bottom, by means of pressure regulators connected to an UPS station and a two-way bubbler. Hexafluoroethane is non-flammable and it has limited toxicity, when below 1000 ppm level and for short exposure time [ref to be added]. In case of a major damage of the

Component	QA station 1	QA station 2	QA detail and backup
Aerogel	Temple U.	BNL	INFN-BA
Gas	BNL		INFN-TS
Mirror	JLab		Duke U.
Sensor (SiPM)	INFN CS-SA-CT	INFN-TS	INFN-BO
Readout	INFN-BO	INFN-FE	INFN-TO

Table 8.2: Planned quality assurance (QA) stations, organized in order to provide redundancy and support specific characterization studies.

supply pipeline or of the vessel itself, 12 m^3 of hexafluoroethane at atmospheric pressure from the vessel (0.02% of the hall volume) will mix with the air present in the experimental hall, requiring the implementation of standard ODH procedures. Hexafluoroethane has a high Global Warming Potential (GWP): 12400 for a horizon time of 100 years [15] and it is, therefore, included in the group of GreenHouse Gasses (GHG). Environment protection imposes that GHGes are not released in the atmosphere. This is obtained by using them in closed circuits, where leakages are minimized, and by collecting and sending for disposal the fraction of gas purged during circuit filling and gas recovery at the beginning and at the end of an operation period, respectively. Both closed circuit gas circulation and purged gas trapping are characterizing elements of the dRICH radiator gas system design. The maximum expected leakage rate during operation is about 20 m^3 / year assuming six-month operation. Experience in quality assurance protocols has being gained in parallel with the R&D activity. For each critical component two stations are being organized to provide essential QA and redundancy, with a (third) station able to supports in-deep characterization on samples and serve as backup, see Table 8.2. The QA activity will be supported by manpower from all the dRICH groups. Essential QA parameters will be measured: integrity, refraction index, transparency, dimensions, and planarity of the aerogel; leak rate of the gas system (after completion); refractive index and transparency of the radiator gas (with the monitoring equipment of the gas system); dark count rate and PDE for the sensors; electrical connections, bias levels and data rate for the readout; dimensions, weight, reflectivity and D0 (point-like source image brigthness) for the mirrors.

Annealing of SiPM will be performed during technical stops and/or during the annual stops of the EIC machine. All the dRICH front-end electronics (FEE) will not be powered, with the exception of a few components needed to monitor and control the annealing operations. An interlock-based sistem will inhibit the FEE power-supply units during annealing. The circulating thermostat system used to cool the SiPMs will be switched to heating mode to reach a temperature of up to T = 100°C. A slow heating ramp of < 1 °C/minute will be employed to reduce thermal stress on the system. The dRICH photodetector boxes will be thermally insulated as much as possible to reduce heat leaks into neighbouring detectors while performing annealing. It is expected that the inner volume of the detector box can reach a temperature of T = 100°C and will be monitored with temperature sensors. Temperature sensors will be placed on the outside of the photodetector boxes to monitor the external environment. Annealing of the whole dRICH photosensors at once requires up to 160 kW of power and will not be performed as such. Only a fraction of the dRICH SiPMs will perform annealing at a given time, to limit the total amount of power needs to about 20-40 kW. This is a similar to the total power consumption of the FEE during normal operations and the same safety procedures apply. Annealing power will be distributed evenly across the dRICH SiPM. In case of a power outage, the annealing current will be promptly removed from the SiPMs and their temperature will promptly drop to the temperature of the thermostat. The latter will eventually slowly cool down.

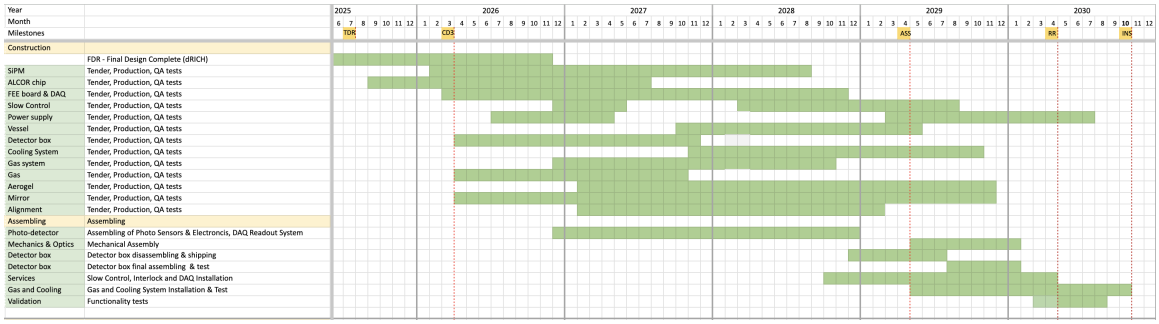

Figure 8.20: Construction plan

Construction and assembly planning:
The construction and assembling plan assumes to compress all the necessary tasks in a short time period in between the presently known EIC milestones: start with CD3 (at the beginning of 2026) and completion 6 months in advance of installation (in October 2030). This results in an aggressive schedule in terms of manpower and funding profile. The 6 months contingency time before installation will be used to perform functionality tests, and complete the services in the experimental hall at IP6. The assembling of 1248 PDUs comprising SiPM sensors and cooling, front-end electronics and RDOs, and their integration with the services inside six detector boxes will be staged over 2 years (mainly 2027 and 2028) by the dRICH DSC in Italy. This organized effort requires a timely procurement, starting with the ALCOR chip (wafer and packaging) followed by sensors, readout electronics, and box mechanics. Cooling infrastructure and DAQ system are expected to run in parallel to the detector box construction and be mainly covered by the EIC Project. First articles of DAQ, power supply and slow control could be used for the initial functionality tests of each single detector box, but the main effort on such services is concentrated on a later stage of the plan during assembling at BNL. The detector boxes will be completed in time to be shipped to BNL and mounted on the dRICH in the second half of 2029. The dRICH vessel construction, a joint venture of the dRICH DSC and the EIC Project, will start in 2028 in order to be ready for detector assembling mid 2029. Mirror production is expected to take 2 years and is staged as soon as possible, subject to the funding profile of the EIC Project, to reduce the sole source risk. The engineering of the aerogel production is expected to extend beyond the TDR, with the consequent production led by the dRICH DSC not happening before 2027 and lasting for at least 2.5 years. An early procurement of the C_2F_6 gas by the EIC Project is planned in order to reduce the risk of a market price increase. The principle design of the radiator gas system will be completed by the end of 2026 by the dRICH DSC. The executive drawings and the system realization by the EIC Project engineering team supported by adequate technical personnel is expected during years 2027 and 2028. The layout finalization and validation of the monitoring equipment will be completed by the end of 2026, while its realization is by the end of 2027 by the dRICH DSC. This equipment will be interfaced with the gas system in 2028, via synergistic effort between the EIC Project engineering team and the dRICH DSC. This combined group will perform the QA assessment of the gas system in 2029.

Collaborators and their role, resources and workforce:
INFN has agreed on a substantial in-kind contribution and the corresponding workforce has taken corresponding responsibilities in the construction within the DSC. The INFN in-kind will cover the design, production and quality assurance cost of the SiPM sensors, of front-end ASIC (ALCOR), of the front-end board (FEB), of the readout boards (RDO) as well as the assembly of the above components in a compact Photo Detector Unit (PDU), including the cooling circuitry and related

mechanics. It will cover the cost of the realization of the six detector boxes (containing the PDU of each sector) with the control panels and the electronic services attached (for HV/LV/daq links routing). It will contribute to the design and realization of the main vessel, the design/supervision of the powering and monitoring systems, the dRICH tagging system and data filtering in streaming mode, see Sec. **??** , and to the definition of specifications and quality assurance (QA) of all the other components and services (i.e. gas, power and cooling plants). The availability of the essential local resources as mechanical and electronic workshops and laboratory space have been negotiated. **INFN-FE** (IT): is coordinating the DSC activity and is leading the mechanical design. The group will lead the design and production of the vessel in collaboration with the EIC Project and will take care of the realization of the detector boxes and corresponding control panels for the 6 sectors. The assembly of the detector boxes is expected to happen in its laboratories. **INFN-BO** (IT): the group is leading the activity on photosensors (SiPM) and data-acquisition. It will be responsible of the procurement of SiPM, design and production the readout boards (RDO) and coordinate the integration of the various elements of the PDU. The PDU will be assembled in BO and tested/validated before being moved to INFN-FE for the installation in the detector boxes. **INFN-BA** (IT): the group is leading the aerogel activity. It will coordinate the mass production and the quality assurance (expected to be operated in the US at Temple University and BNL). **INFN-CS-SA-CT** (IT): this cluster of units will work on the QA of SiPM and front-end boards prior of the PDU assembling. They will equip test stations in SA and CS for this purpose. **INFN-GE** (IT): is carrying out a feasibility study (and if successful, the realization) of an interaction tagger to filter the dRICH data stream. **INFN-LNS** (IT): the group will contribute to the mechanical design effort. **INFN-RM1/RM-TV** (IT): the RM1 group (and one staff person of RM-TV) has extensive experience on AI algorithm running on FPGA. They will develop algorithm for pattern recognition and data reduction on FELIX cards and the interface with the signals received by the dRICH tagger or from ePIC via GTU. **INFN-TO** (IT): the group is leading on the design, test and production of the front-end ASIC ALCOR. The group will produce the chips and the front-end cards (FEB) mounting the ALCOR, and coordinate the quality assurance tests of the chip and FEB. **INFN-TS** (IT): the group is leading the radiator gas activity. It will lead the design of the gas system and develop a continuous monitor system (critical to maintain a good chromaticity). It will also develop a test station of SiPM (with smaller capacity with respect to the CS-SA-CT cluster). **DUKE U.** (US) is leading the mirror activity. It will coordinate the mirror production, expected to happen in the States, the corresponding QA activity, and the coating process that possibly will be realized at Stony Brook. **Jefferson Lab** (US) is contributing to the mechanical design and developing tools for mirror characterization. **Brookhaven Lab** (US) is contributing to the mechanical design and integration study. It will lead the infrastructure (installation tools, services, safety control) realization with its design authority and technical resources. **Stony Brook** (US) is developing mirror coating capability. **Temple U.** (US) is developing an aergel quality assurance facility. **M.S.Ramaiah U.** (India) is contributing to the simulation and performance study. **NISER** (India) is contributing to the performance study. **Haryana and Karnataka U.** (India) have started contrinuting to the performance study. Secondments of personnel from all the DSC groups will be organized to support the QA activity in US and the assembling phase at BNL. The EIC Project is expected to cover the procurement effort that can be more efficiently based on US, and all the safety, infrastructural and integration aspect that require specific engineering background. This include the cost of the gas, of the mirrors, of the installation tools, of the power-supply systems , of the cooling plant and the gas plant, and of the FELIX cards receiving the data from the RDO.

Risks and mitigation strategy:
The major risk of the dRICH gas radiator is the banning of the hexafluoroethane or more severe restriction on its usage, that can also result in increased cost or difficult procurement. The only alternative option to preserve the dRICH performance would be an eco-friendly gas with very

similar refractive index, an option not available in nature at atmospheric pressure. Argon at ≈ 3 bar absolute pressure mimics with great accuracy the hexafluoroethane characteristics. It is also non-expensive, non-toxic and non-flammable. R&D is being performed within the EIC generic R&D program to establish the validity of this approach as risk mitigation strategy. Radiation damage reduces the lifetime of the SiPM as good photodetector for the dRICH performance. Estimates of the radiation level on the dRICH photodetectors are expected to be accurate. The DCR model shown in Figure 8.8 (right) is for the sensors experiencing the largest radiation levels (closer to the beam line) and for detector operation at V_{over} = 4 V and T = -30°C. Operation at lower V_{over} = 3 V and/or lower temperature T = -40°C would reduce the DCR without loss in performance, hence allowing one to accommodate larger integrated radiation levels (up to a factor 2-3) than those reported in the figure. The addition of small thermoelectric cooling (TEC) modules will be evaluated as a potential approach to boost the cooling performance, allowing one to reach an even lower operation temperature of T = -50°C and avoid possible dishomogeneities. Current R&D on new SiPM technologies for improved performance and radiation hardness are being followed up as a risk mitigation strategy and as a potential upgrade for the dRICH photodetector in the late 2030's or in the early 2040's. For two components, optical aerogel and carbon-fiber mirror, there is only one known supplier able to deliver the wanted specifications at the present stage. An early procurement should limit the risk of a market discontinuity. Within the ePIC RICH Consortium, the recently initiated R&D on mirrors at Purdue University are being followed up as potential sources of risk mitigation in the long term period, if the adaptation to the dRICH needs will be proven feasible. DSC members are part of the recent DRD4 initiative, that aims to create a worldwide collaborative environment to favor new technological breakthroughs in Cherenkov particle identification and photon detectors. Within DRD4, there are many development areas of interest for the dRICH program, in particular gasses or mixtures alternative to the greenhouse fluorocarbon gasses and radiation hard SiPM.

Additional Material Planning of additional material for the gas radiator system/monitoring equipment:

- Radiator Aerogel:
  - aerogel characterization in lab and beam tests;
  - details of the aerogel support and purging;
- Radiator Gas:
  - Hexafluoroethane characteristics;
  - Detailed description of the gas system;
  - Options for gas separation during filling and gas recovery operations;
  - Trapping system to collect hexafluoroethane in the purged gas;
  - Jamin interferometer for refractive index measurement;
  - Measurement of the transparency with the spectrophotometer;
  - Oxygen and water vapor contamination: measurement and removal;
  - High-pressure Ar R&D;
- Mirror:
  - mirror characterization in lab and beam tests;
  - details of the mirror structure;
  - details of the mirror support;
  - details of the mirror alignment;

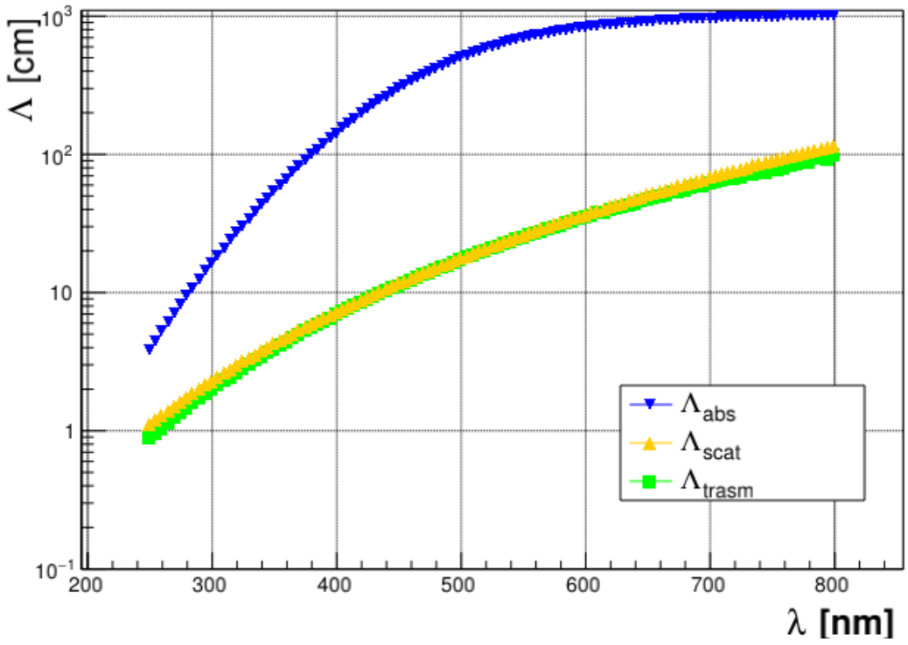

Figure 8.21: Transmission, absorption and scattering length curves as a function of the wavelength for the tile with $n = 1.03$.

In the following the specifications of the main dRICH components are tabulated.

Detector element	Abbreviation	Elements/sector	Total elements
Photodetector box	PDB	1	6
Master panel board	MPB	26	156
Photodetector unit	PDU	208	1248
Silicon photomultiplier	SiPM	53248	319488
SiPM sensor arrays		832	4992
Readout board	RDO	208	1248
Front-end board	FEB	832	4992
ALCOR chips		832	4992

Table 8.3: Main elements of the dRICH photodetector system with the indication of number of elements per sector and the total.

Parameter	Value	Notes
Package type	SiPM array	
Package dimension	$< 26 \times 26$ cm^2	
Mounting technology	surface mount	
Number of channels	64	
Matrix layout	8×8	
Channel size	3×3 mm^2	
Fraction of active area in package	$> 85\%$	
Microcell pitch	50 - 75 μm	
Protective window material	silicone resin	radiation & heat resistant
Protective window refractive index	1.55 - 1.57	
Spectral response range	300 to 900 nm	
Peak sensitivity wavelength (λ_{peak})	400 - 450 nm	
Photon detection efficiency at λ_{peak}	$> 40\%$	
Breakdown voltage (V_{break})	< 60 V	
Operating overvoltage (V_{over})	< 5 V	
Operative voltage (V_{op})	< 64 V	
Max V_{op} variation between channels	< 100 mV	at T = -30°C
Channel dark count rate (DCR)	< 50 kHz	
DCR at T = -30°C	< 5 kHz	at T = -30°C
DCR increase with radiation damage	< 500 kHz/10^9 n_{eq}	at T = -30°C
Residual DCR after annealing	< 50 kHz/10^9 n_{eq}	at T = -30°C
Terminal capacitance	< 500 pF	
Gain	$> 1.5\ 10^6$	
Recharge time constant (τ)	< 100 ns	
Crosstalk (CT)	$< 5\%$	
Afterpulsing (AP)	$< 5\%$	
Operating temperature range	-40 to 25°C	
Single photon time resolution (SPTR)	< 200 ps FWHM	

Table 8.4: Baseline specifications of the SiPM sensor devices for the dRICH photodetector. All parameters are defined at room temperature (T = 25°C) and at the operating voltage V_{op}, unless otherwise specified.

Tile	Refractive index @405 nm	Nominal thickness (mm)
1	1.03	20.7
2	1.03	20.8
3	1.03	20.1
4	1.03	20.5
5	1.03	20.4
6	1.03	10.0
7	1.03	10.0
8	1.04	20.3
9	1.04	20.5
10	1.04	20.3
11	1.04	20.4
12	1.04	20.5
13	1.05	20.5
14	1.05	20.7
15	1.05	20.6
16	1.05	20.6
17	1.05	20.8
18	1.005	20.0
19	1.005	20.0
20	1.005	20.0

Table 8.5: Tiles list. Tiles from 1 to 17 were produced at the High Energy Accelerator Research Organization (KEK) in Japan and delivered in March 2021 [2], except tiles 6-7 which belongs to a 2000 production manufactured by Matsushita Electric Works (Japan).

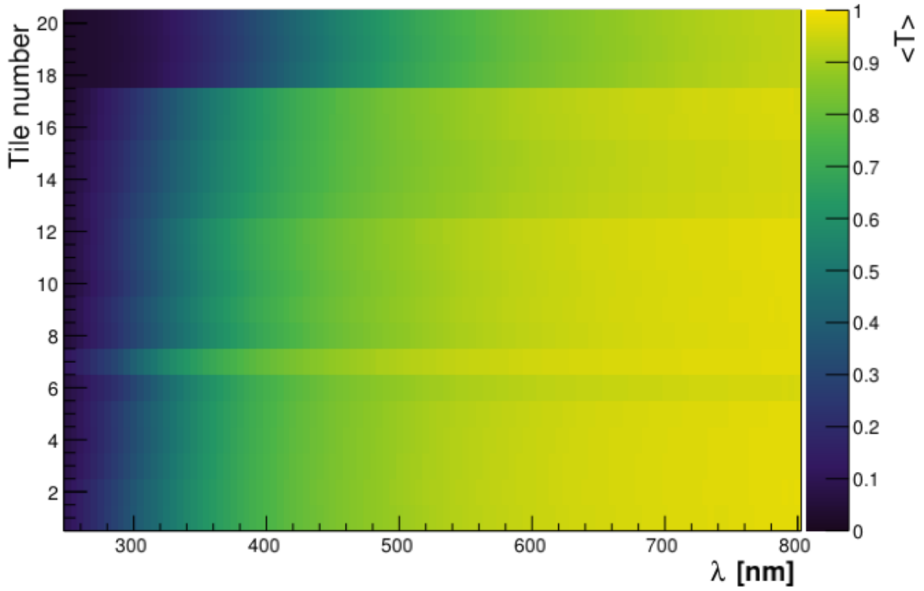

Figure 8.22: Transmittance as a function of the wavelength for all the tiles.

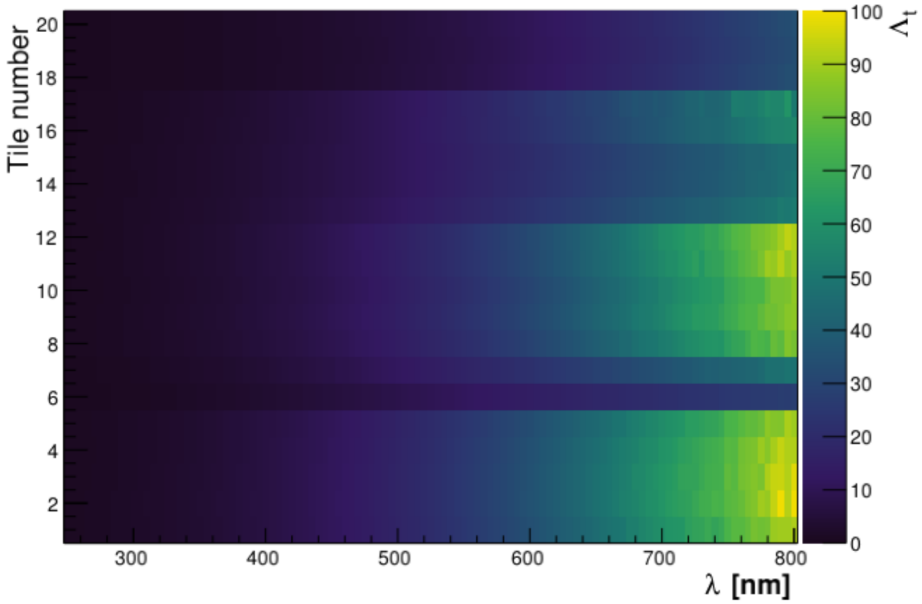

Figure 8.23: Transmission length as a function of the wavelength for all the tiles.

8.3.3 Readout Electronics and Data Acquisition

Requirements

Requirements from physics: Add text here.

Requirements from Radiation Hardness: Add text here.

Requirements from Data Rates: Add text here.

Justification

Device concept and technological choice: Add text here.

Subsystem description:

General device description: Add text here.
Sensors: Add text here.
FEE: Add text here.
Other components: Add text here.

Implementation

Services: Add text here.

Subsystem mechanics and integration: Add text here.

Calibration, alignment and monitoring: Add text here.

Status and remaining design effort:

R&D effort: Add text here.
E&D status and outlook: Add text here.
Other activity needed for the design completion: Add text here.
Status of maturity of the subsystem: Add text here.

Environmental, Safety and Health (ES&H) aspects and Quality Assessment (QA planning: Add text here.

Construction and assembly planning: Add text here.

Collaborators and their role, resources and workforce: Add text here.

Risks and mitigation strategy: Add text here.

Additional Material Add text here.

8.3.4 Software and Computing

Requirements

Requirements from physics: Add text here.

Requirements from Radiation Hardness: Add text here.

Requirements from Data Rates: Add text here.

Justification

Device concept and technological choice: Add text here.

Subsystem description:

General device description: Add text here.

Sensors: Add text here.

FEE: Add text here.

Other components: Add text here.

Implementation

Services: Add text here.

Subsystem mechanics and integration: Add text here.

Calibration, alignment and monitoring: Add text here.

Status and remaining design effort:

R&D effort: Add text here.

E&D status and outlook: Add text here.

Other activity needed for the design completion: Add text here.

Status of maturity of the subsystem: Add text here.

Environmental, Safety and Health (ES&H) aspects and Quality Assessment (QA planning: Add text here.

Construction and assembly planning: Add text here.

Collaborators and their role, resources and workforce: Add text here.

Risks and mitigation strategy: Add text here.

Additional Material Add text here.

8.4 Detector Integration

Add text here.

8.4.1 Installation and Maintenance

Add text here.

8.5 Detector Commissioning and Pre-Operations

Add text here.

References

[1] M. Tabata *et al.*, "Silica aerogel radiator for use in the A-RICH system utilized in the Belle II experiment," *Nucl. Instrum. Meth. A*, vol. 766, pp. 212–216, 2014.

[2] M. Tabata, I. Adachi, H. Kawai, T. Sumiyoshi, and H. Yokogawa, "Hydrophobic silica aerogel production at kek," *Nuclear Instruments and Methods in Physics Research Section A: Accelerators, Spectrometers, Detectors and Associated Equipment*, vol. 668, pp. 64–70, 2012.

[3] S. K. Sahu *et al.*, "Measurement of Radiation Damage on Silica Aerogel Cherenkov Radiator," *Nucl. Instrum. Meth. A*, vol. 382, pp. 441–446, 1996.

[4] R. Abjean, A. Bideau-Mehu, and Y. Guern, "Refractive index of hexafluoroethane (C-2F-6) in the 300-nm to 150-nm wavelength range," *Nucl. Instrum. Meth. A*, vol. 354, pp. 417–418, 1995.

[5] C. Piemonte and A. Gola, "Overview on the main parameters and technology of modern Silicon Photomultipliers," *Nucl. Instrum. Meth. A*, vol. 926, pp. 2–15, 2019.

[6] L. P. Rignanese, P. Antonioli, R. Preghenella, and E. Scapparone, "SiPMs and examples of applications for low light detection in particle and astroparticle physics," *Riv. Nuovo Cim.*, vol. 47, no. 5, pp. 299–349, 2024. [Erratum: Riv.Nuovo Cim. 47, (2024)].

[7] R. Hawkes, A. Lucas, J. Stevick, G. Llosa, S. Marcatili, C. Piemonte, A. Del Guerra, and T. A. Carpenter, "Silicon photomultiplier performance tests in magnetic resonance pulsed fields," in *2007 IEEE Nuclear Science Symposium Conference Record*, vol. 5, pp. 3400–3403, 2007.

[8] S. España, L. Fraile, J. Herraiz, J. Udías, M. Desco, and J. Vaquero, "Performance evaluation of sipm photodetectors for pet imaging in the presence of magnetic fields," *Nuclear Instruments and Methods in Physics Research Section A: Accelerators, Spectrometers, Detectors and Associated Equipment*, vol. 613, no. 2, pp. 308–316, 2010.

[9] F. Acerbi *et al.*, "Cryogenic Characterization of FBK HD Near-UV Sensitive SiPMs," *IEEE Trans. Electron. Dev.*, vol. 64, pp. 521–526, 10 2016.

[10] S. Merzi, F. Acerbi, C. Aicardi, D. Fiore, V. Goiffon, A. G. Gola, O. Marcelot, A. Materne, and O. Saint-Pe, "Radiation Damage on Silicon Photomultipliers from Ionizing and Non-Ionizing Radiation of Low-Earth Orbit Operations," *Sensors*, vol. 24, no. 15, p. 4990, 2024.

[11] E. Garutti and Y. Musienko, "Radiation damage of SiPMs," *Nucl. Instrum. Meth. A*, vol. 926, pp. 69–84, 2019.

[12] T. Tsang, T. Rao, S. Stoll, and C. Woody, "Neutron radiation damage and recovery studies of SiPMs," *JINST*, vol. 11, no. 12, p. P12002, 2016.

[13] R. Preghenella *et al.*, "Study of radiation effects on SiPM for an optical readout system for the EIC dual-radiator RICH," *Nucl. Instrum. Meth. A*, vol. 1056, p. 168578, 2023.

[14] E. Nappi, "Aerogel and its applications to rich detectors," *Nuclear Physics B - Proceedings Supplements*, vol. 61, no. 3, pp. 270–276, 1998. Proceedings of the Fifth International Conference on Advanced Technology and Particle Physics.

[15] EU, "Regulation (EU) 2024/573 of the European Parliament and of the Council on fluorinate greehouse gases," *https://eur-lex.europa.eu/eli/reg/2024/573/oj*, 2024.